# Optimization of combustion parameters of carbonized rice husk briquettes in a fixed bed using RSM technique

P. Kipngetich[a], R. Kiplimo[ab], J. K. Tanui[c1] and P. C. Chisale[d]

a Pan African University Institute for Basic Sciences, Technology and Innovation, P. O. Box 62000-00200 Nairobi

b Department of Marine Engineering and Maritime Operation, Jomo Kenyatta University of Agriculture and Technology, P.O. Box 62000 – 00200 Nairobi, Kenya

c Department of Mechanical Engineering, Dedan Kimathi University of Technology Private Bag 10143, Nyeri, Kenya.

d Department of Mechanical Engineering, The Copperbelt University, 4662 Jambo Drive, Riverside Campus, P. O. Box 21692, Kitwe, Zambia.

## Abstract

This study investigates the combustion of carbonized rice husk briquettes in a fixed bed in order to establish the optimum briquetting and combustion conditions. The combustion properties, namely, the average flame propagation speed, the average burning rates, the reaction zone thickness, maximum flame temperature and the ignition time, were optimized with respect to air-flow rate, binder ratio and particle size using surface response methodology (RSM). Seventeen experiments with different combinations of air-flow rate, binder ratio, and particle sizes, each at three levels set according to Box–Behnken Design (BBD), a RSM technique, were performed. Mathematical models for predicting the responses were developed by fitting experimental data. It was established that the binder and air-mass flux predominantly affected all fuel samples during processing and combustion. Optimal values of the ignition time and reaction zone thickness were established to be 249.08 s and 102.43 mm when air-mass flux, binder ratio and particle size were 0.31 kg/m$^2$.s, 25% and 2.6 mm, respectively. On the other hand, the optimal peak flame temperature were 1226.35 $^0$C when air-mass flux, binder ratio and the particle size were 0. 31 kg/m$^2$.s, 25 % and 0.3 mm, respectively.

*Keywords:* Fixed bed; Briquette combustion; Rice husks briquettes; Box–Behnken design; Response surface methodology; Optimization

[1] Corresponding Author.
Email address: josephat.tanui@dkut.ac.ke; Phone: +254723503095 (J.K. Tanui)

## 1. Introduction

Alternative renewable energy sources are currently being sought as the world stares at an immediate future characterized by energy crises and environmental degradation. At the same time, energy use in Africa is growing two times faster than in most of the world. Only 2 % of $CO_2$ emissions from the world's energy use come from Africa, but the continent is disproportionately affected by that 2 % [1]. The advent of non-conventional energy technologies has attracted considerable research interest globally. As one of them, biomass contributes more than 14 % worldwide [2]. The benefits of biomass energy utilization include carbon neutrality, affordability and sustainability [3].

In sub-Saharan Africa, charcoal production stands at 65 % of the world's output, with 40 % exported to Europe for the barbecue market [4, 5]. Therefore, there is a need to consider utilizing other biomass sources such as agricultural wastes, municipal solid wastes, and energy crops to reduce deforestation and ensure environmental conservation. Further, with the projected over-population in Africa, anthropogenic activities are likely to put high pressure on the forestal biomass. In Kenya, rural households currently use over 90 % of the country's energy demand, with firewood and charcoal reporting an average of 4.5 million tons annually [6]. The over-reliance on forest biomass has led to the loss of water catchment areas and subsequent reduction in water levels in Kenyan rivers and dams, which form the primary sources of electricity.

In Kenya, agriculture is the primary source of revenue which contributes 24 % of Gross Domestic Product (GDP) [7]. According to Kimutai *et al*. [7], Kenya can generate an energy capacity of approximately 187,000 TJ, equivalent to 13,913,223 tons of agricultural residues annually. Globally, Ajimotokan *et al*. [2] project the future production capacity of agricultural residues to reach $2 \times 10^{12}$ tons annually. Agricultural waste is thus often readily available, accessible, and sustainable. They can be processed into pelletized fuels to replace diminishing forest biomass.

Production of pellet fuels from agricultural waste, in many instances, requires a binder to improve its compactness. Researchers have used cassava starch and clay [8], sugar cane molasses [6], carboxymethyl cellulose and calcium lignosulfonate [9] previously as binders- which leads to enhanced physical and chemical properties of pelletized fuels. These additives help extend durability, and they trap the particles by forming elements that are non-evaporative. However, the non-combustible properties of some binders, such as kaolin binders, reduce the calorific value of

the pelletized fuels [2]. The quantity of binders used affects the density and, consequently, the overall performance of the biofuel. Flame front velocity and specific fuel consumption are also affected by the fuel ratio to the binder. Low-density biomass fuels have higher flame front velocity than high-densities since low packing in low-density fuels favours high reactivity and effective penetration of the radiative heat [10].

Currently, pellets and briquettes are commonly produced through low and high compaction pressure methods. The high compaction method is costly in comparison to the low-pressure techniques. Under high compaction, production begins by first adding water and then pressing the biomass at high pressure and temperature through a hydraulic press or a reciprocating piston within a mold. According to Holubcik *et al*. [11], the densification procedure includes; separation, crushing, drying, pelleting, cooling, storage and transporting. A more commonly used approach to densify agricultural residues in Africa is briquetting and pelleting under low pressure (< 7 MPa), where agricultural wastes are first carbonized and a binder is added before densification to enhance cohesion [12]. This process can be achieved with a screw extruder, in which the contributions from electricity, thermal and chemical energy are usually minimal. Biomass, during carbonization, is transformed to carbon by pyrolysis at high temperatures (> 400 $^0$C) and low oxygen supply. Carbon enrichment approaches coal as the temperatures increase, leading to higher HHV than the original biomass. Low-pressure densification methods are favoured because they are less expensive and use readily accessible resources- perfect for African farmers, youth, and women groups.

Biomass combustion in a fixed bed is influenced by several factors, which have been broadly categorized into fuel morphology, fuel composition, and operating conditions [13]. Several authors have independently investigated factors in each category to establish how they impact the combustion process in fixed beds. According to Mahapatra [14], it is not easy to draw a conclusion based on individual factors because they greatly depend on each other. Flame propagation, for instance, is affected by air-flow, combustion and heat transfer. Still, it depends on the porosity, the fuel density, particle size, thermal conductivities, calorific values, moisture and ash contents [14].

Pelletized fuels are often processed by incorporating binders which are typically non-combustible materials. Biomass combustion furnaces and boilers are accompanied by exacerbated corrosion, agglomeration and fouling problems. These conditions result in inadequate air-fuel mixing, reduced thermal efficiency and incomplete combustion due to failure to reach the ignition

temperature. Carbon and hydrogen may not be completely oxidized to carbon dioxide and water, resulting in the formation of deadly carbon monoxide. Such challenges have been identified to encourage the extra costs of combustion chamber cleaning and maintenance. Pelletized fuels have not been fully explored in a fixed bed to analyze the effects of binders on individual biofuel, focusing on burning rate, air-flow rates, temperature profiles, emissions, and flame speed under air/fuel conditions. These combustion properties can be used to characterize biomass fuels with excellent ignitability, less ash contents, improved energy densities among other desirable fuel properties. Furthermore, there is need for optimization of briquette combustion with respect to binder amount and burning conditions.

The main aim of this work was to optimize the combustion properties of carbonized rice husk briquettes in a fixed bed with respect to binder ratio, air-flow rate and particle size using response surface methodology. Box–Behnken Design (BBD) approach was used to investigate the interaction of the three factors to establish suitable combustion conditions and fuel properties that offer high efficiencies with better energy densities. Furthermore, using analysis of variance (ANOVA) and regression analysis (R.A.), the independent factors that provide the best combustion properties in terms of the average flame propagation speed, the average burning rates, the reaction zone thickness, maximum flame temperature and the ignition time were obtained. Consequently, a mathematical model was developed to predict these combustion properties as a function of the input parameters.

## 2. Methodology

### 2.1 Briquette Production Process

Rice husks used in this study were obtained from rice growers in Mwea, Kirinyaga County, central Kenya. Sugarcane molasses binders were purchased locally from Juja town in Kiambu County, Kenya. The dried raw rice husks materials were fed into a carbonizer consisting of a 200 L volume capacity steel drum (2:1 height to diameter ratio) with air regulating holes of 0.02 m in diameter to make biochar. The raw rice husks were fired from the top of the carbonizer drum, then the drum's lid was closed to prevent the raw material from escaping. The holes were filled with mud to minimize the amount of air available for the predicted pyrolytic reaction in the carbonizer. The procedure was held for 4 hours, and the carbonization temperature was kept below 400 $^{0}$C throughout. The sample preparation began by threshing the biomass before sieving. The particle

sizes were sieved using 0.6 mm,1.25 mm, 1.7 mm and 3.5 mm sieves. The mean of the various particle sizes in each category was assumed for this study, i.e., 0.3 mm, 0.9 mm, 1.5 mm and 2.6 mm. Samples of fuels with these sizes is shown in Fig. 1(a)-(d).

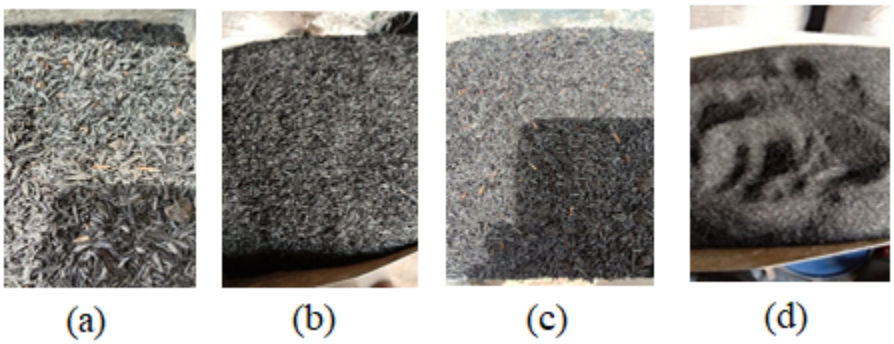


Figure 1: Carbonized rice husks; a) 2.6mm b) 1.5mm c) 0.9mm d) 0.3mm.

A briquetting machine with a screw extruder, available at JKUAT's Mechanical Department, was utilized to make cylindrical briquettes with 38 mm diameters, as illustrated in Fig. 2(a). The briquettes were cut into 40 mm parts, by length, for all the samples produced. Samples of briquettes produced at 35 wt% binder ratio and 1.5 mm particle size are shown in Fig. 2(b). In this paper, pure carbonized rice husks are considered. The chosen percentage for the molasses binder's variation was set between 25 and 45 wt%. The homogeneity and uniformity in the husks/molasses mixing process were achieved by diluting with water (10 % of the total mixture).

**2.2 Fuel Sample Properties**

Moisture content (MC) of different fuel samples produced was determined according to CEN-TS 14774-2:2009 standard. The gross calorific value, volatile matter (V.M.) and the ash contents (A.C.) were determined using the CEN-TS 14918:2009, CEN-TS 15148:2009 and CEN-TS 4775:2009 standards, respectively. The fixed carbon (F.C.) was determined by difference.

(a) (b)

Figure 2: Briquette production process: (a) Briquette Making Machine and (b) samples of briquettes produced at 35 wt% binder ratio and 1.5 mm particle size.

**2.3 Experimental Set-Up**

All experiments were conducted on a fixed-bed experimental rig, as shown in Fig. 3. Five components form the rig system: the fixed-bed reactor, the temperature data acquisition system, the emission sampling system, the fuel mass weighing scale and the air-flow monitoring apparatus. The combustion device consists of a vertical cylinder combustion chamber measuring 750 mm high and 160 mm inside diameter. The chamber is designed and built of four material layers: the inner layer of the furnace wall, a 40 mm thick refractory cement with thermal conductivity of 0.86 W/m.K [15], a 2 mm thick mild steel plate and an 18 mm thick insulation material made of aluminium silicate cotton fiber. According to Lienhard and John [15], the thermal conductivity of aluminium silicate cotton fiber is 0.055 W/m.K at lower temperatures up to 400 K. The typical convective heat transfer coefficient values, h, for air in natural convection of 10-20 $W/m^2.K$ [16] was chosen for this study. Thus, having considered designing for the critical thickness of insulation of the fixed bed a 276 mm outer radius was sufficient for heat insulation in this reactor.

The air was supplied via a perforated bottom plate. The plate was made of 1Cr18Ni9Ti stainless steel and could withstand temperatures of up to 1400 $^0C$. There were 66 grate holes, each 10 mm in diameter. The plenum was made circular and sealed to reduce turbulence and minimize air leakages.

The fuel combustion chamber was weighed using a WT1503L electronic scale to determine the mass-loss history. With the help of an RS232 cable, weight data on the scale were transferred to an excel database installed on the computer. Tubes were made with flexible connections to minimize the effect of weight on the scale. Nine Type-K thermocouples (TC) with measurement ranges of about 0 to 1360 $^0$C were put into the chamber to monitor temperature at 50 mm intervals and provide the velocity of propagation of the various reaction fronts (drying, devolatilization, or char oxidation). A data logging device (BTM-4208SD) with an accuracy and resolution of 0.4 $^0$C and 0.1 $^0$C respectively, was used to record temperature values after every 10 seconds from 9 different channels. The air-flow rate was determined using LZB–25 and LZB–100 type float flow meters with ranges of 1–25 m$^3$/h and 20–100 m$^3$/h, respectively, with an error of ±0.2 m$^3$/h.

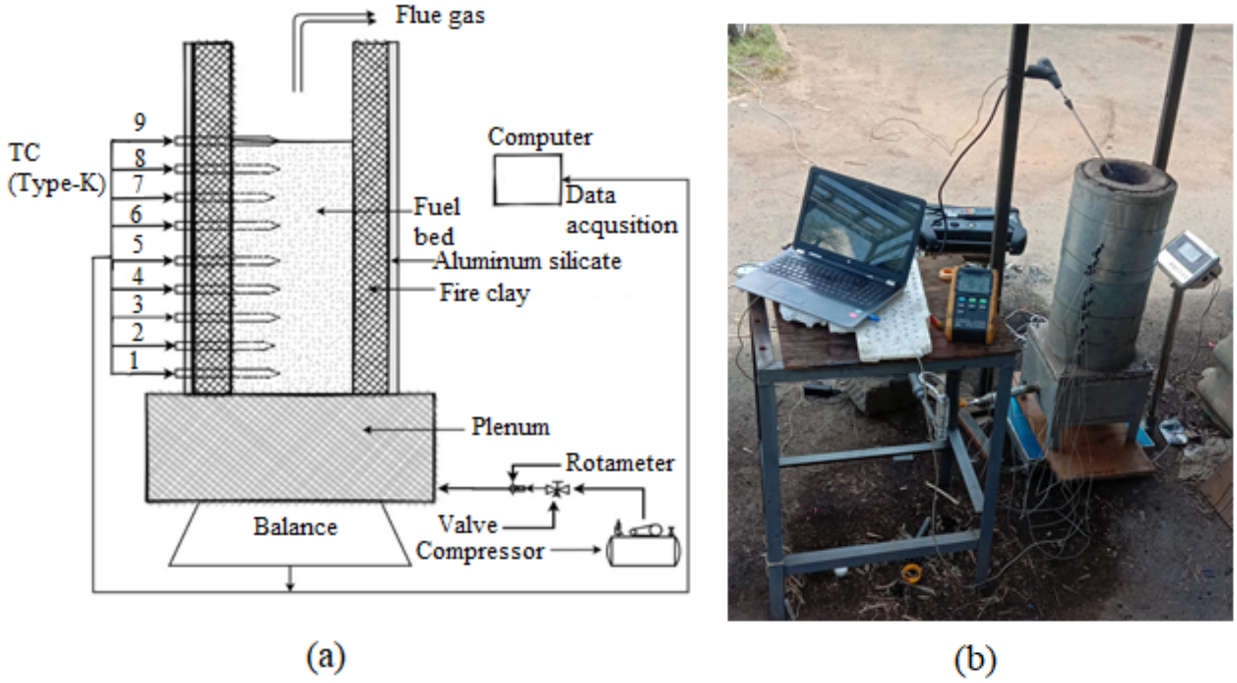


Figure 3: Experimental set-up: (a) schematic diagram and (b) photo of laboratory set-up.

### 2.4 Determination of Combustion Properties

#### 2.4.1 Average Flame Propagation Speed

The average flame propagation speed, $u_{fps}$ was determined using the distance between adjacent thermocouples, $\Delta x$ and the time between the occurrence of the peak temperatures in the adjacent thermocouples, $(\Delta t)_f$, as expressed through Eq. (1).

$$u_{fps} = \frac{\Delta x}{(\Delta t)_f} \#(1)$$

### 2.4.2 Ignition Time

It is a property of the fuel, which refers to the time taken for the reaction front to begin at the top surface of the fuel bed. It varied for different fuel samples due to different molasses binder levels and the particle size used before densification. The ignition time, $t_{ig}$ is the time when there is a sharp increase in flame temperature as indicated in Fig. 4.

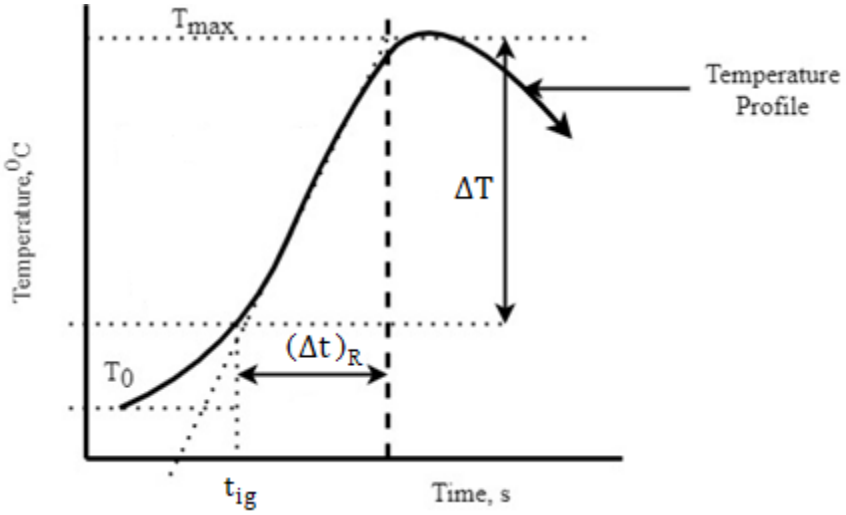


Figure 4: Diagram illustrating reaction zone thickness determination from temperature profiles

### 2.4.3 Reaction Zone Thickness

The reaction zone thickness, $x_R$ was evaluated based on the temperature profiles generated. This represents the overall thickness of a reaction zone measured as the axial distance from the point where the bed temperature rises from ambient temperature to its maximum value, as shown in Fig. 4. Assuming a steady state flame propagation, the reaction zone thickness from each thermocouple position was obtained by the time difference between the point where the temperature starts to rise sharply to the maximum value, $(\Delta t)_R$, and the average flame propagation speed as shown in Eq. (2). The average reaction zone thickness was obtained by averaging the reaction zones thickness from all thermocouples.

$$x_R = u_{fps}(\Delta t)_R \#(2)$$

### 2.4.4 Burning Rate

The burning rate, $\dot{m}_b$ (kg/m$^2$.s) is the mass consumption of the fuel over a given period. It is normalized by the cross-sectional area of the fuel bed, *A*. The burning rate is complete when there is no further mass loss and the temperature has reduced significantly. Eq. (3) outlines a method that gives the values for the aggregated process average; for both the devolatilization phase and the char oxidation period.

$$\dot{m}_b = \frac{1(\Delta m)_{dc}}{A\,(\Delta t)_{dc}} \#(3)$$

where $(\Delta m)_{dc}$, and $(\Delta t)_{dc}$ are the total mass of fuel consumed and time during devolatilization and char oxidation phases, respectively.

### 2.5 Design of Experiments

This study utilized the Box–Behnken Design (BBD) approach to determine the optimum binder ratio, air-flow rate, and particle sizes. BBD methodology, a response surface methodology (RSM), lowered the cost and number of experiments and helped in establishing optimum values of combustion properties [17, 18]. The number of experiments in three-level factorial BBD is calculated as $N = 2\,k(k-1)\,+\,cp$, where *cp* is the number of central points, *k* is the number of factors, and *N* is the number of experiments.

As a result, the total number of experiments in this research was 17, with 12 experiments for each factor at three levels and five centre experiments. All variables were changed at three equally spaced levels (-1, 0, + 1), as required by BBD. The binder ratio, the air-mass flux and the particle size were coded as $x_1$, $x_2$ and $x_3$, respectively. The three levels of these factors are presented in Table 11. Design-Expert 13 software package was used to generate the experimental points as per BBD methodology. The experimental data was used to determine the regression model and the data are shown in Table 2.

Furthermore, ANOVA was used to evaluate the statistical significance of the regression model. ANOVA results from the response variables investigated are shown in Table 3. The binder ratio, the air-mass flux and the particle size are represented as A, *B* and *C*, respectively, in the design expert software.

Table 1:Physical and coded values for input factors

| Input Factors | Coded values of input factors | | |
|---|---|---|---|
| | $x_{i,min}$ | $x_{i,0}$ | $x_{i,max}$ |
| | (-1) | (0) | (+1) |
| Binder ratio, wt% (A) | 25 | 35 | 45 |
| Air-mass flux, kg/m$^2$.s (B) | 0.02 | 0.31 | 0.6 |
| Particle size, mm (C) | 0.3 | 1.5 | 2.6 |

Table 2: Combustion properties of sample fuels as a function of input factors

| Samples | Air - mass flux | Binder ratio | Particle size | Average flame propagation speed | Average burning rate | Ignition Time | Reaction Zone Thickness | Peak Flame Temperature |
|---|---|---|---|---|---|---|---|---|
| | kg/m$^2$. s | wt% | mm | mm/s | kg/m$^2$.s | sec | mm | $^0$C |
| 1 | 0.6 | 35 | 2.6 | 0.0629 | 0.0141 | 315 | 81.91 | 960.64 |
| 2 | 0.02 | 45 | 1.5 | 0.0571 | 0.0126 | 330 | 48.88 | 843.02 |
| 3 | 0.31 | 35 | 1.5 | 0.0776 | 0.0144 | 255 | 84.28 | 1162.29 |
| 4 | 0.31 | 35 | 1.5 | 0.0775 | 0.0145 | 255 | 84.18 | 1166.29 |
| 5 | 0.31 | 35 | 1.5 | 0.0769 | 0.0146 | 250 | 82.38 | 1162.29 |
| 6 | 0.6 | 25 | 1.5 | 0.0682 | 0.0142 | 305 | 78.15 | 998.22 |
| 7 | 0.31 | 45 | 0.3 | 0.0723 | 0.0137 | 320 | 77.24 | 1125.02 |
| 8 | 0.6 | 45 | 1.5 | 0.0548 | 0.0141 | 335 | 73.43 | 961.58 |
| 9 | 0.02 | 25 | 1.5 | 0.0639 | 0.0135 | 295 | 64.38 | 879.65 |
| 10 | 0.31 | 25 | 2.6 | 0.0913 | 0.0152 | 250 | 102.43 | 1125.65 |
| 11 | 0.31 | 35 | 1.5 | 0.0771 | 0.0144 | 255 | 84.19 | 1162.29 |
| 12 | 0.31 | 25 | 0.3 | 0.0804 | 0.0143 | 265 | 76.95 | 1224.98 |
| 13 | 0.31 | 45 | 2.6 | 0.0799 | 0.0145 | 280 | 81.85 | 1153.78 |
| 14 | 0.02 | 35 | 2.6 | 0.0644 | 0.013 | 305 | 63.95 | 855.54 |
| 15 | 0.02 | 35 | 0.3 | 0.0524 | 0.0123 | 340 | 45.01 | 880.27 |
| 16 | 0.31 | 35 | 1.5 | 0.0776 | 0.0145 | 260 | 83.32 | 1160.29 |
| 17 | 0.6 | 35 | 0.3 | 0.0547 | 0.0132 | 340 | 68.3 | 1010.52 |

Table *3*:ANOVA results for all responses

| Source | Response: Average flame propagation speed | | | | | Response: Burning rate | | | | | Response: Ignition Time | | | | |
|---|---|---|---|---|---|---|---|---|---|---|---|---|---|---|---|
| | Sum of Squares | df | Mean Square | F-value | Prob> F | Sum of Squares | df | Mean Square | F-value | Prob> F | Sum of Squares | df | Mean Square | F-value | Prob> F |
| Model | 0.002 | 9 | 0.0002 | 1487 | < 0.0001 | 9.76E-06 | 9 | 1.08E-06 | 167.2 | < 0.0001 | 18988 | 9 | 2110 | 147.1 | < 0.0001 |
| A | 1.10E-06 | 1 | 1.10E-06 | 7.35 | 0.0301 | 2.19E-06 | 1 | 2.19E-06 | 338.31 | < 0.0001 | 75 | 1 | 75 | 5.25 | 0.0557 |
| B | 0.0002 | 1 | 0.0002 | 1309 | < 0.0001 | 6.58E-07 | 1 | 6.58E-07 | 101.53 | < 0.0001 | 2851 | 1 | 2851 | 198.81 | < 0.0001 |
| C | 0.0002 | 1 | 0.0002 | 1254 | < 0.0001 | 1.36E-06 | 1 | 1.36E-06 | 209.94 | < 0.0001 | 1653 | 1 | 1653 | 115.26 | < 0.0001 |
| AB | 0 | 1 | 0 | 72.97 | < 0.0001 | 1.60E-07 | 1 | 1.60E-07 | 24.68 | 0.0016 | 6 | 1 | 6 | 0.4358 | 0.5303 |
| AC | 3.56E-06 | 1 | 3.56E-06 | 23.84 | 0.0018 | 1.04E-08 | 1 | 1.04E-08 | 1.61 | 0.2452 | 26 | 1 | 26 | 1.78 | 0.224 |
| BC | 2.75E-06 | 1 | 2.75E-06 | 18.39 | 0.0036 | 2.18E-09 | 1 | 2.18E-09 | 0.3366 | 0.58 | 162 | 1 | 162 | 11.27 | 0.0121 |
| $A^2$ | 0.0016 | 1 | 0.0016 | 10572 | < 0.0001 | 4.89E-06 | 1 | 4.89E-06 | 753.93 | < 0.0001 | 12165 | 1 | 12165 | 848.13 | < 0.0001 |
| $B^2$ | 0 | 1 | 0 | 256.9 | < 0.0001 | 1.64E-07 | 1 | 1.64E-07 | 25.33 | 0.0015 | 237 | 1 | 237 | 16.51 | 0.0048 |
| $C^2$ | 2.88E-06 | 1 | 2.88E-06 | 19.32 | 0.0032 | 2.31E-07 | 1 | 2.31E-07 | 35.69 | 0.0006 | 1027 | 1 | 1027 | 71.6 | < 0.0001 |
| Residual | 1.05E-06 | 7 | 1.49E-07 | | | 4.54E-08 | 7 | 6.48E-09 | | | 100 | 7 | 14 | | |
| Lack of Fit | 6.33E-07 | 3 | 2.11E-07 | 2.05 | 0.2499 | 1.74E-08 | 3 | 5.80E-09 | 0.828 | 0.5435 | 50 | 3 | 17 | 1.34 | 0.3787 |
| Pure Error | 4.12E-07 | 4 | 1.03E-07 | | | 2.80E-08 | 4 | 7.00E-09 | | | 50 | 4 | 13 | | |
| Cor Total | 0.002 | 16 | | | | 9.80E-06 | 16 | | | | 19088 | 16 | | | |
| | | | | | | | | | | | | | | | |
| Source | Response: Reaction Zone Thickness | | | | | Response: Peak Flame Temperature | | | | | | | | | |
| | Sum of Squares | df | Mean Square | F-value | Prob> F | Sum of Squares | df | Mean Square | F-value | Prob> F | | | | | |
| Model | 3101.8 | 9 | 344.64 | 539.2 | < 0.0001 | 2.75E+05 | 9 | 30525.8 | 7521.4 | < 0.0001 | | | | | |
| A | 795.34 | 1 | 795.34 | 1244.3 | < 0.0001 | 2.80E+04 | 1 | 28007.2 | 6900.8 | < 0.0001 | | | | | |
| B | 195.87 | 1 | 195.87 | 306.45 | < 0.0001 | 2.83E+03 | 1 | 2834.7 | 698.5 | < 0.0001 | | | | | |
| C | 490.47 | 1 | 490.47 | 767.36 | < 0.0001 | 2.63E+03 | 1 | 2634.7 | 649.2 | < 0.0001 | | | | | |
| AB | 29.05 | 1 | 29.05 | 45.45 | 0.0003 | 0.00E+00 | 1 | 0.0 | 0.0 | 0.9981 | | | | | |
| AC | 7.27 | 1 | 7.27 | 11.37 | 0.0119 | 1.58E+02 | 1 | 157.5 | 38.8 | 0.0004 | | | | | |
| BC | 108.77 | 1 | 108.77 | 170.18 | < 0.0001 | 4.10E+03 | 1 | 4095.8 | 1009.2 | < 0.0001 | | | | | |
| $A^2$ | 1463.3 | 1 | 1463.3 | 2289.5 | < 0.0001 | 2.35E+05 | 1 | 235000.0 | 57950.2 | < 0.0001 | | | | | |
| $B^2$ | 5.89 | 1 | 5.89 | 9.21 | 0.019 | 1.38E+02 | 1 | 138.2 | 34.0 | 0.0006 | | | | | |
| $C^2$ | 0.0468 | 1 | 0.0468 | 0.0732 | 0.7946 | 6.47E-01 | 1 | 0.6 | 0.2 | 0.7015 | | | | | |
| Residual | 4.47 | 7 | 0.6392 | | | 2.84E+01 | 7 | 4.1 | | | | | | | |
| Lack of Fit | 1.78 | 3 | 0.595 | 0.885 | 0.5208 | 9.21E+00 | 3 | 3.1 | 0.6 | 0.6285 | | | | | |
| Pure Error | 2.69 | 4 | 0.6723 | | | 1.92E+01 | 4 | 4.8 | | | | | | | |
| Cor Total | 3106.3 | 16 | | | | 2.75E+05 | 16 | | | | | | | | |

## 3. Results and Discussion

### 3.1 Effects of Binders on Fuel Properties

The binder significantly affects the thermal properties of biomass fuels under investigation, as illustrated in Table 4-6. In this research, the values of volatile matter ranged between 14.09-20.04 %. They were generally lower than those reported by Kerich et al. [20] for carbonized rice husks because of the high proportions of molasses binders used in this study. An increase in molasses binders leads to a reduction in the calorific value of the fuel. This, as well, may be attributed to the presence of non-combustible volatiles in molasses [6].

The carbonized rice husks' volatile matter should be lower than raw rice husks' [8]. Low values are a result of the loss of some volatiles during carbonization. The enhanced ignition properties of fuel samples from carbonized rice husks and reduced smoke during their utilization position them better than fossil fuels. A small amount of energy is needed to evaporate the little moisture content present in the fuel samples. Compared to the literature review, the below 40 % volatile matter in these fuel samples justifies their suitability for domestic and industrial applications [19]. All the samples burnt for a long time without spark, soot, and were smokeless.

The calorific values ranged between 16.4 and 23.71 MJ/kg. The values are lower than those registered in other studies because of low volatile levels [20] and excessively high ash levels. The molasses binders used were more than those used in other studies [21, 6] making fuels samples more hygroscopic. That property may have led to moisture absorption upon exposure to the environment during utilization.

Table 4: Proximate analysis for briquettes from 1.5 mm particle sizes.

| Molasses, wt% | Ash, % | vm, % | FC, % | Gross CV, MJ/kg |
|---|---|---|---|---|
| 25 | 49.7±0.045a | 15.08±0.0116a | 32.43±0.128a | 22.54±0.809a |
| 30 | 50.35±0.166b | 16.45±0.0023b | 29.63±0.028b | 22.29±0.200b |
| 35 | 51.09±0.002c | 17.82±0.0003c | 26.8275±0.001c | 22.038±0.000c |
| 40 | 51.72±0.007d | 18.77±0.0300d | 24.51±0.095d | 20.96±0.241d |
| 45 | 52.63±0.033e | 19.72±0.1751e | 21.91±0.475e | 19.88±0.988e |
| p-value | 0.032 | 0.056 | 0.046 | 0.053 |

Table 5: Proximate analysis for briquettes from 0.3 mm particle sizes.

| Molasses, wt% | Ash, % | vm, % | FC, % | Gross CV, MJ/kg |
|---|---|---|---|---|
| 25 | 48.88±0.001a | 26.51±0.034a | 21.58±0.032a | 26.36±0.021a |
| 30 | 49.44±0.048b | 24.45±0.002b | 22.34±0.042b | 24.55±0.006b |
| 35 | 49.72±0.073c | 22.65±0.000c | 22.55±0.004c | 22.64±0.000c |
| 40 | 50.34±0.079d | 21.71±0.010d | 22.26±0.003d | 21.58±0.040d |
| 45 | 51.55±0.079e | 20.85±0.001e | 22.41±0.167e | 20.88±0.003e |
| p-value | 0.035 | 0.033 | 0.048 | 0.028 |

Table 6: Proximate analysis for briquettes from 2.6 mm particle sizes.

| Molasses, wt% | Ash, % | vm, % | FC, % | Gross CV, MJ/kg |
|---|---|---|---|---|
| 25 | 47.65±0.0774a | 24.54±0.056a | 25.78±0.756a | 21.59±0.062a |
| 30 | 48.34±0.0236b | 23.36±0.066b | 26.16±0.089b | 21.63±0.122b |
| 35 | 48.25±0.393c | 20.98±0.316c | 27.63±0.903d | 20.72±0.033c |
| 40 | 49.32±0.108d | 20.54±0.0651d | 25.67±0.356e | 18.55±0.006d |
| 45 | 49.32±0.337e | 19.8±0.064e | 26.45±0.061f | 16.65±0.076e |
| p-value | 0.031 | 0.046 | 0.048 | 0.023 |

*The data presented in Tables 4-5 are the mean values of four replicates. Values in the same column with different alphabet are significantly different at α =0.05 using Duncan multiple range test.*

### 3.2 Overall Effects of Briquette Processing and Combustion Conditions on Combustion Properties

#### 3.2.1 Bed Temperature Profiles

Temperatures profiles in the fixed bed for various combination of air mass flux, binder ratio and particle sizes are shown in Fig. 5( a-d). In all the graphs. the combustion of biomass adopts a specific profile outlining two stages of combustion in a fixed bed. The two phases are characterised by two peak temperatures for the corresponding phases. The first phase which is due to ignition of the biomass leads to a rapid rise in bed temperature as the ignition front arrives while the second phase results from char oxidationin the fixed bed after a prolonged combustion period.

The maximum bed temperatures have been noted to be greatly influenced by the three input factors chosen for this study. As shown in Fig. 5 (a), maximum bed temperature was highest, 1163 $^0$C; the air-mass flux, binder mass and particle size was 0.31 kg/m$^2$.s, 35 % and 1.5 mm. It's under these conditions that the ignition time was shortest at 250 s similar to the ignition time achieved when binder ratio was reduced to 25 % and particle size increased to 2.6 mm as shown in Fig. 5(d). Fig. 5 (c) had the lowest bed temperature at 880 $^0$C with longest ignition time of 340 s compared

to those indicated in the other graphs. The difference in peak temperatures is attributed to different conditions of maximum air-flow rate, the binder ratios and the particle sizes used during fuel processing.

The graphs also indicate difference in the flame front propagation speeds. This is deduced from the shortest time (4755 s) it took the flame front to move from T9 to T1 in Fig. 5 (d) compared to the longest time (7755 s) in Fig. 5(c).

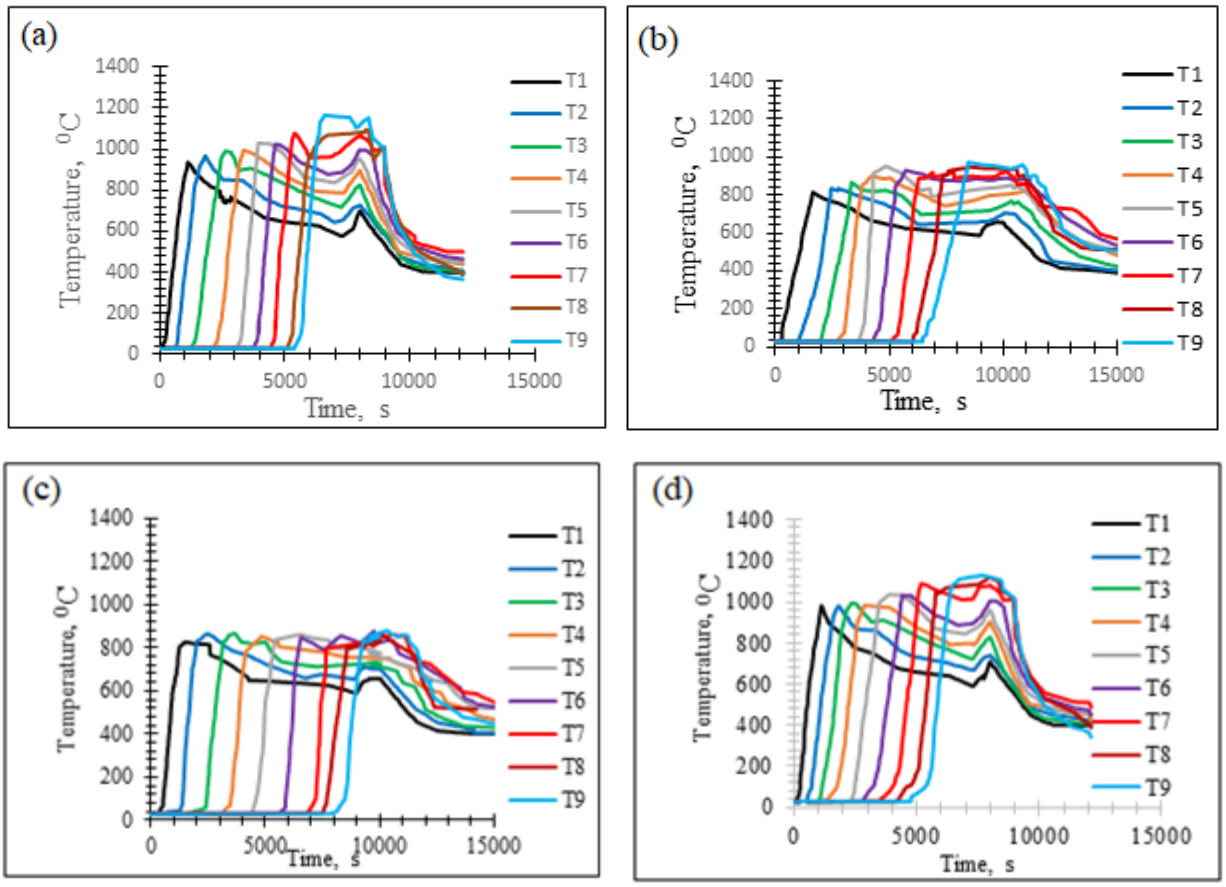


Figure 5: Temperature profiles at different input factors: (a) 0.31 kg/m$^2$.s air mass flux, 35% binder ratio and 1.5 mm particle size, (b) 0.6 kg/m$^2$.s air mass flux, 35% binder ratio and 2.6 mm particle size, (c) 0.02 kg/m$^2$.s air mass flux, 35% binder ratio and 0.3 mm particle size and (d)) 0.31 kg/m$^2$.s air mass flux, 25% binder ratio and 2.6 mm particle size.

### 3.2.2 Average Flame Propagation Speed

The average flame propagation speeds, $u_{fps}$ obtained in the experiments ranged between 0.0524 mm/s and 0.0913 mm/s. The values were estimated at 500 $^0$C as the temperature measurement at different locations along the length of the reactor indicated well establishedtemperature profile at this temperature. At this temperature, the particles react steadily with the incoming gaseous species to form the products of combustions. The heterogeneous reactions with homogenous heat release coupled with devolatilization of the fuel occur [22], and flame propagation is almost uniform at this temperature. Table 3 indicates that the average flame propagation speed' significant model terms are the A, B, C, AB, AC, BC, $A^2$, $B^2$ and $C^2$. The equation governing this combustion property is given by Eq. (4);

$$u_{fps} = 0.093004 + 0.167996A - 0.002326B + 0.005784C - 0.000569AB - 0.002826AC - 0.000072BC - 0.230172A^2 + 0.000030B^2 + 0.000627C^2 \quad \#(4)$$

The predicted $R^2$ of 0.9946 is in reasonable agreement with the adjusted $R^2$ of 0.9988. Fig. 6(a)-(c) show a graphical representation of average flame propagation speed for interaction of the three factors. Shown in Fig. 6 (b), for instance, is a graph of flame propagation speed as a function of binder ratio and air-mass flux when particle size is held constant at 1.5 mm. The graph shows that flame propagation speed increases rapidly from 0.02 kg/m$^2$.s upwards to a peak point at 0.31 kg/m$^2$.s, where it begins to gradually drop to the lowest point at 0.6 kg/m$^2$.s. While carrying out experiments and numerical modeling of the same, using wooden particles, Saastamoinen *et al.* [23] observed that ignition front speed and bed temperature are maximum at a particular critical air flow rate. Further, the propagation speed is inversely proportional to the density of the fuel samples [23]. While using wood, which has less dense bulk density than briquettes used in this study, Mahapatra et al. [35] achieved a peak propagation of 0.083 mm/s at an air-mass flux of 0.12 kg/m$^2$.s. A similar trend was also observed by Dasappa and Paul while using charcoal in their experiments; the peak propagation speed was 0.3 mm/s at an air mass flux of 0.132 kg/m$^2$.s [24]. Shin and Choi [25] observed that the flame propagation speed depends on the calorific value, the particle size and the primary air velocity. Most of the studies indicate that the different propagation speeds at almost the same air-mass fluxes are attributed to the factors such as volatile matter contents, the fixed carbon contents, porosity of the fuel bed, the moisture contents and the calorific values of the fuel [6, 24, 26, 27, 28, 29].

(a)

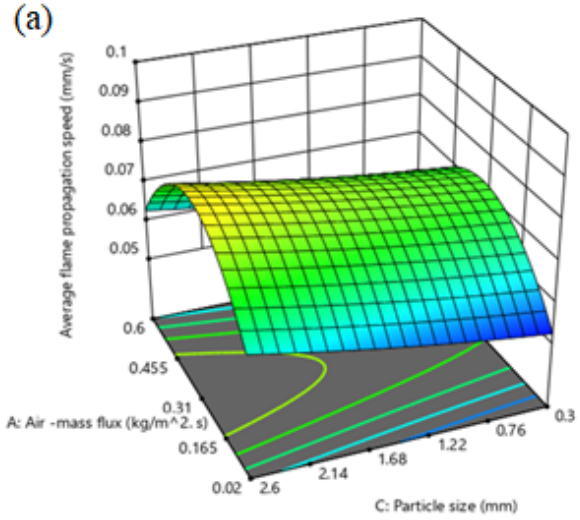


(b)

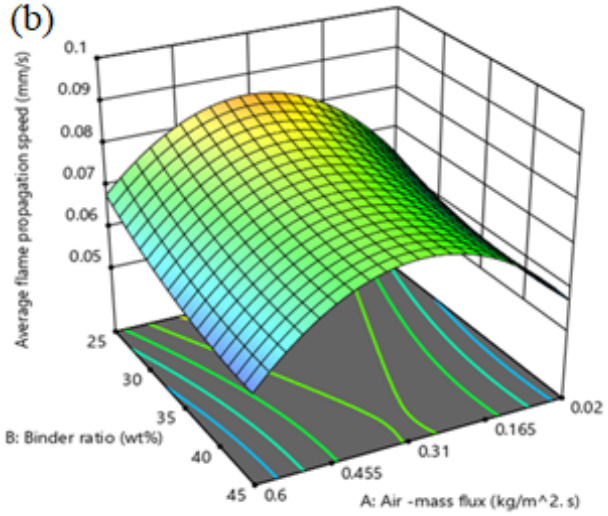

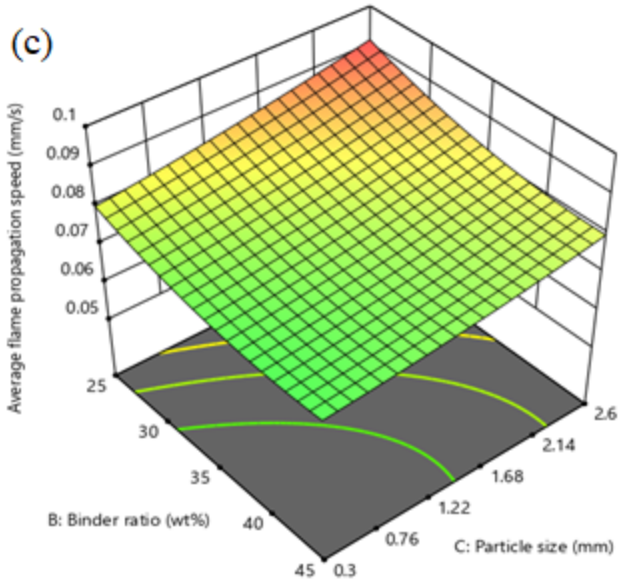


Figure 6: Graphs of average flame propagation speed as a function of binder ratio, particle size and air-mass flux when (a) binder ratio is held constant at 35 wt%, (b) particle size is held constant at 1.5 mm and (c) air-mass flux is held constant at 0.31 kg/m$^2$. s.

### 3.2.3 Average Burning Rate

The burning rate refers to the sum of devolatilization and char combustion rates during the steady-state combustion stage [30]. The average burning rate values for the samples produced ranged between 0.0123 kg/m$^2$.s and 0.0152 kg/m$^2$.s. The factors A, B, C, AB, A$^2$, B$^2$ and C$^2$, were significant model terms for the burning rates as indicated in Table 3. The mathematical model for the average burning rate is shown in Eq. (5);

$$\dot{m}_b = 0.015915 + 0.007114A - 0.000185B + 0.000898C + 0.000069AB - 0.012812A^2 + 1.97500 \times 10^{-6}B^2 - 0.000178C^2 \#(5)$$

The predicted R$^2$ of 0.9672 is obtained and reasonably agrees with the adjusted R$^2$ of 0.9894. Fig. 7(a)-(c) show a graphical representation of average burning rate interaction of the three factors. For this experiment, average burning rate increases rapidly from 0.0123 kg/m$^2$.s when air-mass flux is 0.02 kg/m$^2$.s to a maximum value of 0.0152 kg/m$^2$.s when the air-mass flux is 0.31 kg/m$^2$.s. However, the values obtained in this study are lower because of the high bulk densities of the fuel bed due to densification compared to those of other researchers who used wood chips and other biomass materials [31, 29, 32, 27]. Yang et al. [31] while carrying out combustion of woodchips

and simulation of municipal solid wastes, with primary air-mass flux range of 0.03 kg/m$^2$.s to 0.6 kg/m$^2$.s, observed that the moisture content influences the burning rate. At a given moisture level, Yang et al. [31] report that the burning rates increase to a certain critical air-mass flux level before decreasing gradually. Their maximum values of burning rates were 0.07 kg/m$^2$.s for fuels with 10 % moisture contents and 0.0182 kg/m$^2$.s for 50 % moisture levels.

In this study, as the binder increases, the burning rate decreases. On the other hand, as the particle sizes increases, the porosity is expected to go up and consequently the high burning rate. However, as the particle sizes of the carbonized materials increase, the difference in porosities becomes negligible and consequently, the burning rates at large particle sizes become almost equal. The burning rate trend explains the balance between heat absorbed by fuels during combustion and heat lost due to colder gas streams from the fuel. The increasing average burning rates during low air-mass fluxes are attributed to the high heat generated with less heat carried away by the gas streams. In contrast, the low burning rates at high air-mass fluxes result from the excess gas flow, which takes heat generated by combustion.

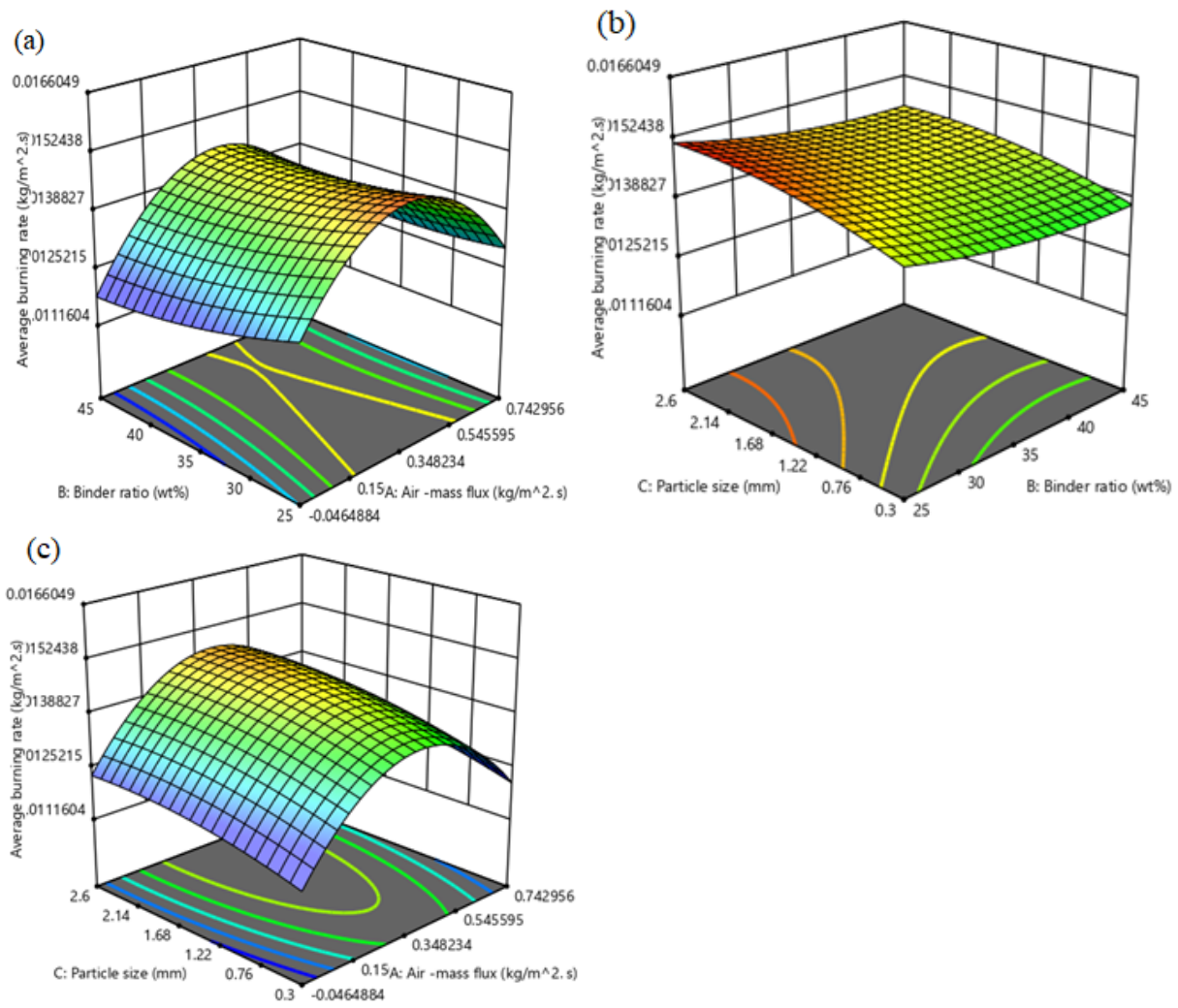


Figure 7: A graph of the average burning rate as a function of binder mass, particle size and air-mass flux when (a) particle size is held constant at 1.5 mm, (b) air-mass flux held constant at 0.31 kg/m$^2$.s and (c) binder ratio held constant at 35 %.

### 3.2.4. Ignition Time

The ignition time, $t_{ig}$ is calculated using measured temperature profiles at various bed heights, assuming a constant flame propagation speed. It is defined as the time when a flame front is formed at the bed surface. The ignition time values of the various sample fuels ranged between 250 seconds and 340 seconds. The model terms that significantly determined the ignition time in the fuel bed were A, B, C, BC, A$^2$, B$^2$ and C$^2$. The A model term was insignificant by 5.57 % and it was not omitted as it supports the mathematical hierarchy. The equation obtained to determine the ignition time is as shown in Eq. (6).

$$t_{ig} = 353.20374 - 381.55899A - 2.42658B - 29.84025C - 0.552408BC + 639.12010A^2 + 0.075000B^2 + 11.83712C^2 \#(6)$$

The predicted $R^2$ values of 0.9537 agree reasonably well with the adjusted $R^2$ of 0.9880. Fig. 8(a)-(c) show interaction of various factors on the ignition time. The graphs indicate that the ignition time increases with increasing air-mass flux up to a critical point that gradually decreases. The values obtained in this study are slightly higher because of high binder amount usage and the densification process, which is not the case with other studies [23, 30]. Yang et al. [30] used biomass samples with moisture contents from 10 % to 50 % and they obtained ignition time in the range of 15 to 560 seconds. Previous researchers have also identified other factors, including the size of fuel, the porosity, material type, primary air flow-rate, energy of the ignition source, bulk density of the bed, and others [30, 14, 22, 14]. In this study, air-mass flux influenced the ignition time significantly. There is the shortest ignition time at sub-stoichiometric conditions since the cooling effect due to excess air is minimum. In this experiment, the shortest ignition time achieved was when the binder used was the least at 25 wt%, the particle size was largest at 2.6 mm, and the air-mass flux was 0.31 kg/m$^2$.s. The longest ignition is achieved at the highest binder mass (45 wt%) with the most increased air-mass flux of 0.6 kg/m$^2$.s. When the air-mass flux was increased past 0.31 kg/m$^2$.s, the combustion time decreased and the time needed for ignition increased.

It was observed that the densities of fuels produced from 0.3 mm particles were higher than that of 2.6 mm particles. The high dense fuel samples, as observed during ignition, exhibited longer ignition times compared to those from larger size particles. This trend results from the high heat energy required to heat a specific volume of the uel bed to the ignition temperature. Less dense materials lose temperature easily through radiation following their smallest heat capacity per unit volume [33].

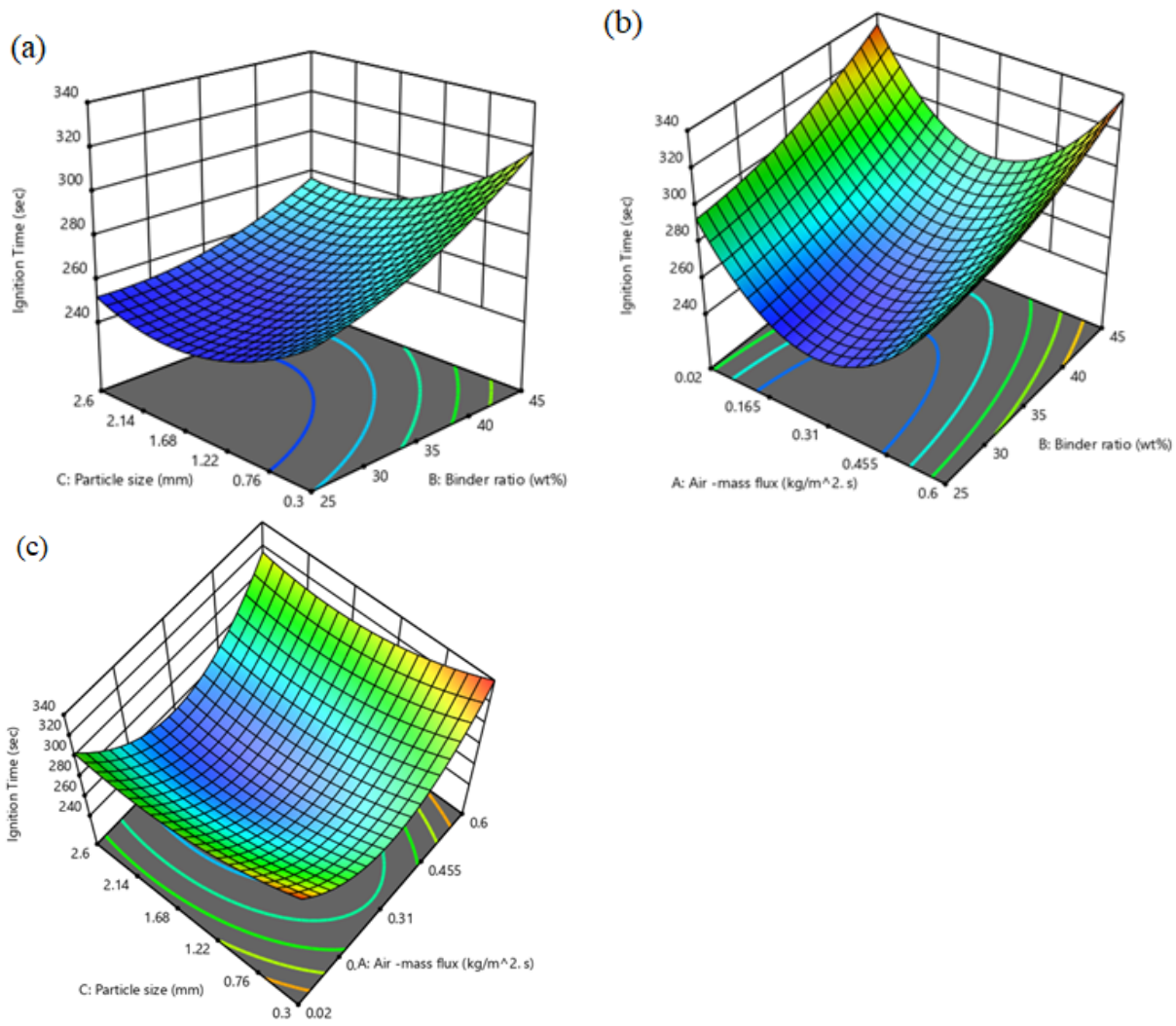


Figure 8: Graphs of ignition time as a function of binder mass, particle size and air-mass flux when (a) air-mass flux is kept constant at 0.31 kg/m$^2$.s, (b) particle size is kept constant at 1.5 mm and (c) binder ratio kept constant at 35 %.

### 3.2.5 Reaction Zone Thickness

The thickness of the reaction zone, $x_R$ is the physical distance in the flame front along which the bed temperature rises from ambient temperature to its maximum value. In this study, average reaction zone thickness values were estimated to lie between 45.01 mm and 102.43 mm. Using cardboard and potatoes as biomass, Yang et al. [33] achieved a reaction zone thickness between 20 mm and 50 mm. The values obtained in this study are slightly higher because of the use of carbonized rice husks, increased sizes of sample fuel and reduced moisture contents. The

significant terms of the model were A, B, C, AB, AC, BC, $A^2$ and $B^2$. Therefore, an equation that can be used to predict the reaction zone thickness was determined by fitting experimental data and it is as shown in Eq. (7).

$$x_R = 58.73647 + 145.16550A - 0.953691B + 23.69248C + 0.929310AB - 4.03943AC - 0.453234BC - 221.67063A^2 + 0.011825B^2 \#(7)$$

The predicted $R^2$ values of 0.9994 agree reasonably well with the adjusted $R^2$ of 0.9998. Shown in Fig. 9(a)-(c) are the interaction of binder mass, air-mass flux and the particle size as they influence the reaction zone thickness when particle size is held constant at 1.5 mm (a), air-mass flux at 0.31 kg/m$^2$.s (b) and binder mass at 35 % (c), respectively. The binder mass significantly affects $x_R$, while particle size portrays little influence. Porteiro et al. [34] observed that the cooling effect increases with the increased air-flow rate; hence, at extremely high air-mass flux conditions, the char particles cool, lowering the energy available to evaporate moisture and release volatiles from the fuel. Therefore, the green fuel bed's heat penetration is limited, resulting in a slight reduction in the reaction front. Reduction in reaction front translates into thinner reaction zone thickness.

According to Yang et al. [35], more combustible mass is packed into a smaller volume for denser fuels. Consequently, the density of the fuel material has the most significant influence on the reaction zone thickness. Denser material gives a thinner reaction zone, which reduces the residence time of the reacting gases. A similar observation has been observed in this study where the sample fuels from smaller particle size (0.3 mm) with low air-mass flux mass (0.02 kg/m$^2$.s) presenting thinner reaction zone thickness. This study's maximum flow rate values (0.6 kg/m$^2$.s) also present a generally thinner reaction zone thickness than those performed at sub-stoichiometric conditions (0.31 kg/m$^2$.s).

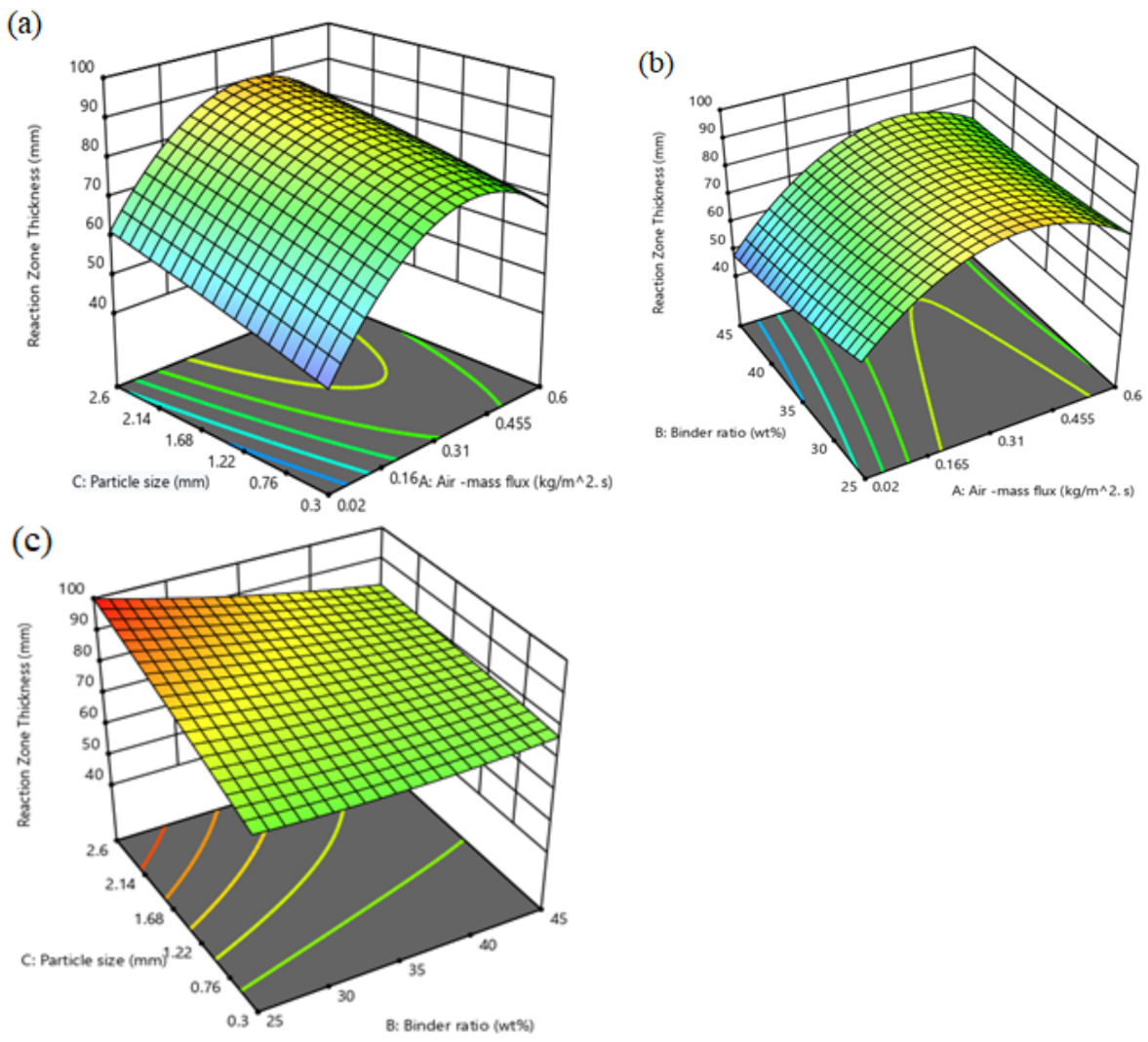


Figure 9: Graphs of reaction zone thickness as a function of binder ratio, air-mass flux and particle size when (a) binder ratio held constant at 35 %, (b) particle size held constant at 1.5 mm and (c) air-mass flux is held constant at 0.31 kg/m$^2$.s.

### 3.2.6 Peak Flame Temperature

The air-mass flux, the particle size and the molasses binder mass significantly influenced the peak flame temperature, $T_{peak}$ within the fuel bed. The peak flame temperatures obtained in this study ranged between 843.02 $^0$C and 1226.35 $^0$C. The identified significant model terms include A, B, C, AC, BC, A$^2$ and B$^2$. The equation for predicting the peak flame temperature in the bed is shown in Eq. (8).

$$T_{peak} = 980.81751 + 1973.79046A - 1.90595B - 106.43194C - 18.80657AC + 2.78124BC - 2810.26707A^2 - 0.057284B^2 \#(8)$$

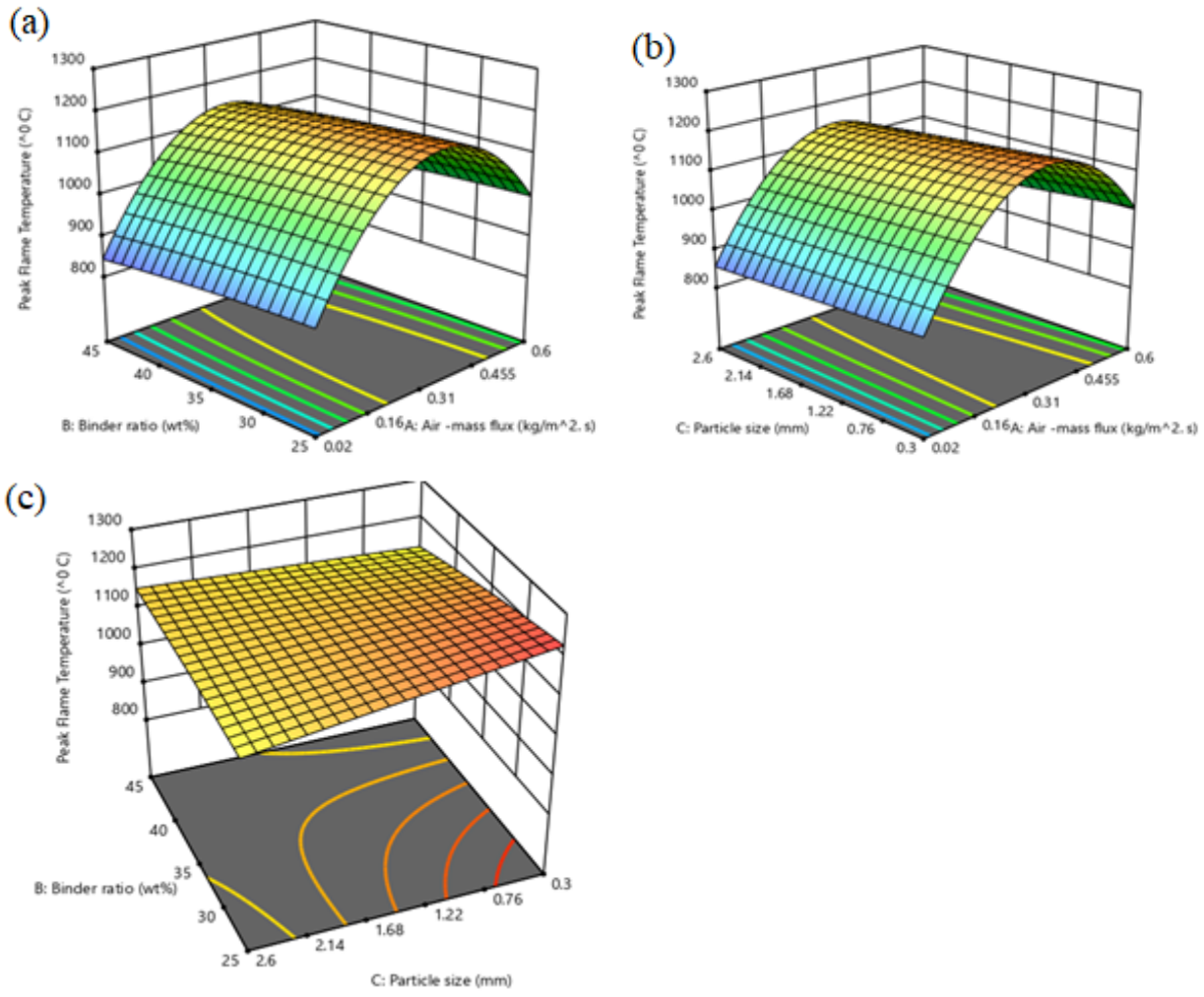


Figure 10: A graph of peak flame temperature as a function of binder ratio, air-mass flux and particle size when (a) particle size held constant at 1.5 mm (b) binder ratio held constant at 35 % and (c) air-mass flux is held constant at 0.31 kg/m$^2$.s.

Shown in Fig.10(a)-(c) is the interaction of the three factor on the flame peak temperature. Maximum flame temperature is obtained at an air-mass flux of 0.31 kg/m$^2$.s; when the particle-sized used for densification is 0.3 mm. The values of flame temperatures obtain compare well with those of other researchers [13, 35]. The flame temperature in the fuel bed is determined by the local ratio of fuel and oxygen supply and reaches a maximum at a given air-flow rate. After that,

increasing the air-flow rate dilutes the gas in the flame, causing the temperature to fall. So, the heat transfer to the virgin fuel is not only by radiation or conduction in the contact points of particles but also through convective heat transfer from flames around the burning fuel.

Finally, optimization was done to determine a combination of these three factors that produced fuel with excellent combustion properties. In this study, the reaction zone thickness, ignition time and the peak flame temperature were chosen as the parameters for optimization to evaluate thermal properties of the briquette while the average flame propagation speed and the burning rates were dropped because of their smaller range. Optimal values of the ignition time and reaction zone thickness were established to be 249.08 s and 102.43 mm when air-mass flux, molasses binder mass and particle size were 0.31 kg/m$^2$.s, 25% and 2.6 mm, respectively. On the other hand, the flame peak optimal temperature values were 1226.35 $^0$C when air-mass flux, molasses binder ratio and the particle size were 0. 31 kg/m$^2$.s, 25 % and 0.3 mm, respectively.

## Conclusion

This study investigated the effects of air-flow rate, binder mass, and particle size on sample fuels' combustion properties. Mathematical models for predicting the average flame propagation speed, the average burning rates, the reaction zone thickness, maximum flame temperature and the ignition time were obtained. The molasses binder predominantly affected the combustion properties of fuels. Increasing the quantity of molasses used resulted in a significant reduction in the flame propagation speed, peak flame temperature and burning rate. However, it led to prolonged ignition times and thinner reaction zone thickness. During fuel processing, therefore, the molasses binder should be kept at a level just sufficient to offer good mechanical properties for proper handling and transportation of fuel. Although the influence of particle size on the fuel's properties was negligible, such as gross calorific value, it proved to be a critical factor that influences the combustion time and the maximum flame temperature. The smallest possible particle sizes during fuel densification leads to fuels with improved calorific values, prolonged burning time and higher flame temperatures. The air-mass flux significantly influences all the combustion properties investigated in this study. In this study, Optimal values of the ignition time and reaction zone thickness were established to be 249.08 s and 102.43 mm when air-mass flux, molasses binder mass and particle size were 0.31 kg/m$^2$.s, 25% and 2.6 mm, respectively. On the

other hand, the flame peak optimal temperature values were 1226.35 $^{0}$C when air-mass flux, molasses binder ratio and the particle size were 0. 31 kg/m$^{2}$.s, 25 % and 0.3 mm, respectively

**Acknowledgement**

This research work was financially supported by Pan African University, Institute for Basic Sciences, Technology and Innovation.

**Data Availability**

Dataset related to this article can be found at http://doi: 10.17632/9mv2hw7kh5.1, an open-source online data repository hosted at Mendeley Data (Tanui et. al., 2022).

**References**

[1] IEA, "International Energy Agency Report," 2019. [Online]. Available: https://www.iea.org/reports/africa-energy-outlook-2019. [Accessed 22 1 2022].

[2] H. A. Ajimotokan, S. E. Ibitoye, J. K. Odusote, O. A. Adesoye and P. O. Omoniyi, "Physico-mechanical properties of composite briquettes from corncob and rice husk," *Journal of Bioresources and Bioproducts,* vol. 4, p. 159–165, 2019.

[3] E. D. Vicente, A. M. Vicente, M. Evtyugina, R. Carvalho, L. A. C. Tarelho, S. Paniagua, T. Nunes, M. Otero, L. F. Calvo and C. Alves, "Emissions from residential pellet combustion of an invasive acacia species," *Renewable energy,* vol. 140, p. 319–329, 2019.

[4] C. Nabukalu and R. Gieré, "Charcoal as an energy resource: Global trade, production and socioeconomic practices observed in Uganda," *Resources,* vol. 8, p. 183, 2019.

[5] J. K. Tanui, P. N. Kioni, T. Mirre, M. Nowitzki and N. W. Karuri, "The influence of particle packing density on wood combustion in a fixed bed under oxy-fuel conditions," *Energy,* vol. 194, p. 116863, 2020.

[6] J. K. Tanui, P. N. Kioni, P. N. Kariuki and J. M. Ngugi, "Influence of processing conditions on the quality of briquettes produced by recycling charcoal dust," *International Journal of Energy and Environmental Engineering,* vol. 9, p. 341–350, 2018.

[7] S. K. Kimutai, A. M. Muumbo, Z. O. Siagi and A. K. Kiprop, "A study on agricultural residues as a substitute to fire wood in Kenya: a Review on Major Crops," *Journal of Energy Technologies and Policy,* vol. 4, p. 45–51, 2014.

[8] M. Lubwama and V. A. Yiga, "Characteristics of briquettes developed from rice and coffee husks for domestic cooking applications in Uganda," *Renewable energy,* vol. 118, p. 43–55, 2018.

[9] W. Yang, Y. Zhu, W. Cheng, H. Sang, H. Xu, H. Yang and H. Chen, "Effect of minerals and binders on particulate matter emission from biomass pellets combustion," *Applied Energy,* vol. 215, p. 106–115, 2018.

[10] W. A. González, F. Zimmermann and J. F. Pérez, "Thermodynamic assessment of the fixed-bed downdraft gasification process of fallen leaves pelletized with glycerol as binder," *Case Studies in Thermal Engineering,* vol. 14, p. 100480, 2019.

[11] M. Holubcik, R. Nosek and J. Jandacka, "Optimization of the production process of wood pellets by adding additives," *International Journal of Energy Optimization and Engineering (IJEOE),* vol. 1, p. 20–40, 2012.

[12] T. H. Mwampamba, M. Owen and M. Pigaht, "Opportunities, challenges and way forward for the charcoal briquette industry in Sub-Saharan Africa," *Energy for Sustainable Development,* vol. 17, p. 158–170, 2013.

[13] J. Porteiro, D. Patiño, J. Moran and E. Granada, "Study of a fixed-bed biomass combustor: influential parameters on ignition front propagation using parametric analysis," *Energy & fuels,* vol. 24, p. 3890–3897, 2010.

[14] S. Mahapatra and S. Dasappa, "Experiments and analysis of propagation front under gasification regimes in a packed bed," *Fuel processing technology,* vol. 121, p. 83–90, 2014.

[15] I. V. Lienhard and H. John, A heat transfer textbook, Phlogiston press, 2005.

[16] F. P. Incropera, A. S. Lavine, T. L. Bergman and D. P. DeWitt, Fundamentals of heat and mass transfer, Wiley, 2007.

[17] B. Lela, M. Barišić and S. Nižetić, "Cardboard/sawdust briquettes as biomass fuel: Physical–mechanical and thermal characteristics," *Waste Management,* vol. 47, p. 236–245, 2016.

[18] M. A. Bezerra, R. E. Santelli, E. P. Oliveira, L. S. Villar and L. A. Escaleira, "Response surface methodology (RSM) as a tool for optimization in analytical chemistry," *Talanta,* vol. 76, p. 965–977, 2008.

[19] M. Lubwama, V. A. Yiga, F. Muhairwe and J. Kihedu, "Physical and combustion properties of agricultural residue bio-char bio-composite briquettes as sustainable domestic energy sources," *Renewable energy,* vol. 148, p. 1002–1016, 2020.

[20] A. Demirbas, "Potential applications of renewable energy sources, biomass combustion problems in boiler power systems and combustion related environmental issues," *Progress in energy and combustion science,* vol. 31, p. 171–192, 2005.

[21] K. D. Kerich, Z. O. Siagi and J. O. Ogola, "Effect of formulation, binder and compaction pressure of rice husk-bagasse briquettes on thermal and physical properties," *Journal of Scientific Research & Reports*, vol. 26(10), p. 38–53, 2020.

[22] B. S. A. Alganash, "Numerical investigation of the combustion processes of various combustion regimes," *PhD thesis, University of Glasgow*, 2015.

[23] J. J. Saastamoinen, R. Taipale, M. Horttanainen and P. Sarkomaa, "Propagation of the ignition front in beds of wood particles," *Combustion and flame,* vol. 123, p. 214–226, 2000.

[24] S. Dasappa and P. J. Paul, "Gasification of char particles in packed beds: analysis and results," *International journal of energy research,* vol. 25, p. 1053–1072, 2001.

[25] D. Shin and S. Choi, "The combustion of simulated waste particles in a fixed bed," *Combustion and flame,* vol. 121, p. 167–180, 2000.

[26] P. McNamee, L. I. Darvell, J. M. Jones and A. Williams, "The combustion characteristics of high-heating-rate chars from untreated and torrefied biomass fuels," *Biomass and bioenergy,* vol. 82, p. 63–72, 2015.

[27] X. Meng, R. Sun, W. Zhou, X. Liu, Y. Yan and X. Ren, "Effects of corn ratio with pine on biomass co-combustion characteristics in a fixed bed," *Applied Thermal Engineering,* vol. 142, p. 30–42, 2018.

[28] X. Meng, W. Zhou, E. Rokni, H. Zhao, R. Sun and Y. A. Levendis, "Effects of air flow-rate on the combustion and emissions of blended corn straw and pinewood wastes," *Journal of Energy Resources Technology,* vol. 141, 2019.

[29] M. Horttanainen, J. Saastamoinen and P. Sarkomaa, "Operational limits of ignition front propagation against air-flow in packed beds of different wood fuels," *Energy & fuels,* vol. 16, p. 676–686, 2002.

[30] Y. B. Yang, H. Yamauchi, V. Nasserzadeh and J. Swithenbank, "Effects of fuel devolatilization on the combustion of wood chips and incineration of simulated municipal solid wastes in a packed bed," *Fuel,* vol. 82, p. 2205–2221, 2003.

[31] Y. B. Yang, V. N. Sharifi and J. Swithenbank, "Effect of air flow rate and fuel moisture on the burning behaviours of biomass and simulated municipal solid wastes in packed beds," *Fuel,* vol. 83, p. 1553–1562, 2004.

[32] S. Mahapatra, S. Kumar and S. Dasappa, "Gasification of wood particles in a co-current packed bed: Experiments and model analysis," *Fuel Processing Technology,* vol. 145, p. 76–89, 2016.

[33] C. Ryu, Y. B. Yang, A. Khor, N. E. Yates, V. N. Sharifi and J. Swithenbank, "Effect of fuel properties on biomass combustion: Part I. Experiments—fuel type, equivalence ratio and particle size," *Fuel,* vol. 85, p. 1039–1046, 2006.

[34] J. Porteiro, D. Patiño, J. L. Miguez, E. Granada, J. Moran and J. Collazo, "Study of the reaction front thickness in a counter-current fixed-bed combustor of a pelletized biomass," *Combustion and Flame,* vol. 159, p. 1296–1302, 2012.

[35] Y. B. Yang, C. Ryu, A. Khor, N. E. Yates, V. N. Sharifi and J. Swithenbank, Effect of fuel properties on biomass combustion. Part II. Modelling approach—identification of the controlling factors," *Fuel,* vol. 84, p. 2116–2130, 2005.